A Kinetic Model of Nano-CaO Reactions with CO_2 in a Sorption Complex Catalyst

S. F. Wu and P. Q. Lan
Dept. of Chemical and Biological Engineering, Zhejiang University, Hangzhou 310027, China

DOI 10.1002/aic.12675
Published online June 10, 2011 in Wiley Online Library (wileyonlinelibrary.com).

This article describes the reactive kinetics of nano-CaO with CO_2 in a sorption complex catalyst. Based on an observation of nano-CaO reaction with CO_2 has a fast surface reaction regime and followed by a slow diffusion-controlled regime, a criterion has been proposed to divide the fast surface reaction regime and the slow diffusion-controlled reaction regime. The kinetics of the fast surface reaction was studied, and a new ion reaction mechanism was proposed. A surface reaction-controlled kinetic model with a Boltzmann equation, $X = X_u - X_u/[1+exp((t-t_0)k/X_u)]$, was developed. Experiments using nano-CaO to react with CO_2 in a fast surface reaction regime within a sorption complex catalyst were performed using thermogravimetric analysis at 773–873 K under a N_2 atmosphere with 0.010–0.020 MPa CO_2. The activation energy of the kinetic model for carbonation is 30.2 kJ/mol, and the average relative deviation of the sorption ratio is less than 9.8%. *AIChE J,* 58: 1570–1577, 2012
Keywords: CO_2 capture, carbonation, kinetics, nano-CaO, sorption complex catalyst

Introduction

Hydrogen is an important raw material in the chemical and petroleum industries and plays a major role in developing economies. Hydrogen is of particular interest because it is also used for the generation of electric power and employs highly efficient fuel cells. Approximately 95% of the H_2 currently produced in the US uses the steam-methane reforming process.[1] The sorption-enhanced reaction process has the advantages of high thermal efficiency, low economic investment and CO_2 capture.[2–5] A reaction sorption-enhanced reaction (ReSER) process is one type of sorption-enhanced reaction process.[6] The key points of the ReSER system are the use of nano-CaO as the reactant with CO_2, a sorption complex catalyst and a circulating fluidized bed system. Nano-CaO has been identified as the most promising reactant because it has a rapid reactivity with CO_2, high reactive sorption capacity, high durability, low decomposition temperature and abundant natural precursors.[7–9] Most importantly, the fast reaction of nano-CaO with CO_2 plays an important role in the ReSER process for hydrogen products.

The chemical reaction of CaO with CO_2, as shown in Eq. 1, is highly exothermic. The reaction rate of CaO with CO_2 affects the reaction rate of the steam methane reforming reaction.[10–12] The reason for the enhanced reforming reaction is that removing the product will break the thermodynamic equilibrium of a reversible reforming reaction according to the Le Chatelier principle. The same result of enhanced reforming is achieved by removing the hydrogen product using hydrogen-selective membranes and by removing CO_2 using the CaO reaction. Removing CO_2 is much more efficient due to the CO_2 amount being only 1/4 of the hydrogen amount, and the heat from the exothermic reaction of CaO with CO_2 provides the heat for the strong endothermic reforming reaction

$$CaO(s) + CO_2(g) \rightarrow CaCO_3(s); \nabla H = -178kJ/mol \quad (1)$$

Correspondence concerning this article should be addressed to S. F. Wu at wsf@zju.edu.cn.

Simulations and experimental evidence demonstrate that a rapid reaction of CaO with CO_2 decreases the CO_2 content and, therefore, enhances the endothermic steam methane reforming reaction.[13,14] A high methane conversion and over 95% hydrogen content can be obtained.[6]

The use of the CaO reaction to capture CO_2 to break the thermodynamic equilibrium limit requires CaO to be regenerated from $CaCO_3$. This regenerated CaO can then be used in the reactor to enhance the steam reforming reaction. Therefore, a reactor-regenerator system is required: the reactor is required for steam reforming and the CaO reaction with the CO_2, while the regenerator is required for regenerating CaO from $CaCO_3$ and recycling it to the reactor. A circulating fluidized-bed reactor regenerator[9,10] is suitable for this requirement (as in modern FCC units), in which the reactor is usually the riser and the regenerator is usually the downer. This situation requires a fast reaction between CaO and CO_2 in the reactor (because of the short residence time due to the fast fluidization) and, similarly, a fast regeneration of $CaCO_3$ in the regenerator. In addition, recent studies have described a circulating fluidized-bed reactor regenerator technology for post-combustion to remove CO_2 from fuel gas using CaO-based sorbents.[15–18] The need for a fast reaction of CaO with CO_2 is a key technique.

Bhatia[19–21] found that the gas–solid reaction of CaO with CO_2 experiences a rapid reaction of CO_2 followed by a slow CO_2 diffusion-controlled reaction through the $CaCO_3$ layer. A previous study[7] on a nano-CaO reaction with CO_2 also showed that the rapid reaction regime is followed by a slow reaction regime. Nano-CaO reacts rapidly with CO_2, as shown in previous studies.[7,8,22] The stability of using nano-CaO-based CO_2 adsorbents was also experimentally studied by Florin[23] and Lu.[24] From the experimental studies, one significant difference between the nano-CaO and micro-CaO reaction with CO_2 is that nano-CaO has much more surface area. Up to 80% of the conversion ratio occurs in the rapid surface reaction regime (within 2 minutes) for nano-CaO. Alternatively, the micro-CaO reaction with CO_2 only contributes 20% of the conversion ratio in the rapid surface reaction regime.[19] However, the reaction kinetics of the nano-CaO reaction with CO_2 have not been quantitatively studied yet. Thus, the study of the fast surface reaction kinetics of CaO with CO_2 is significant.

Many investigations considered the use of CaO obtained from the calcinations of natural minerals, such as limestone and dolomite, for carbonation through the reaction of CaO with CO_2. $CaCO_3$ exists in limestone and dolomite in micrometer-sized particles, and CaO particles of micrometer size are obtained after calcination. Therefore, almost all the models describe the reaction of CaO with CO_2 based on the micro-CaO reaction with CO_2 for a rapid surface reaction regime and a slow diffusion-controlled reaction regime. One of the classical models is the shrinking core model,[25] as shown in Eqs. 2 and 3

$$\text{Chemical reaction control regime } \frac{dX}{dt} = -\frac{KC_{CO2}}{\rho R}(1-X)^{\frac{2}{3}} \quad (2)$$

$$\text{Diffusion control regime } \frac{dX}{dt} = \frac{6DC_{CO2}}{\rho R^2\left[3(1-X)^{-\frac{1}{3}} - 2X\right]} \quad (3)$$

where X is the CaO conversion, K is the reaction rate constant (expressed by the Arrhenius equation), C_{CO2} is the concentration of CO_2, ρ is the density of a CaO particle, R is the radius of a CaO particle, and D is the diffusion coefficient. Based on the simplicity of the shrinking core model, Johnsen[13] utilized the effective diffusion and the external mass-transfer coefficient to modify the model based on their SEM/EDS observations. Because the CaO–CO_2 reaction is sensitive to the pore-size distribution of calcines, Sun[26] developed a new gas–solid model based on discrete pore-size distribution measurements and applied it to the carbonation reaction of CaO to capture CO_2. Sun suggested that the model accurately showed the pore-size distribution evolution and was easier to understand than other distributed-pore-based pore models. However, it is difficult to use because it requires the initial pore-size distribution of the CaO sorbent after calcination.[27]

Another widely used pore model is the random pore model,[19,20] which assumes the pore structure is a network of randomly interconnected pores and can be represented as follows

Chemical reaction control regime

$$\frac{dX}{dt} = \frac{KC_{CO2}S_0(1-X)\sqrt{1-\psi\ln(1-X)}}{1-\varepsilon_0} \quad (4)$$

Diffusion control regime

$$\frac{dX}{dt} = \frac{KC_{CO2}S_0(1-X)\sqrt{1-\psi\ln(1-X)}}{(1-\varepsilon_0)\left[1+\frac{\beta Z}{\psi}\left(\sqrt{1-\psi\ln(1-X)}-1\right)\right]} \quad (5)$$

In Eqs. 4 and 5, K is the rate constant (expressed by Arrhenius equation), C_{CO2} is the concentration of CO_2, S_0 is the initial surface area per unit volume, ε_0 is the porosity, and L_0 represents the initial total pore length in the porous system per unit volume. ψ is a structural parameter

$$\psi = \frac{4\pi L_0(1-\varepsilon_0)}{S_0^2}$$

The disadvantages of this method are the complexity and the need to obtain information about the structural parameters. The models discussed above have been improved considerably by incorporating more details and properties of the adsorbents.[21,27] However, they still fail to describe the kinetics of nano-CaO reactions with CO_2, especially for the rapid reaction regime.

Based on previous experimental results of nano-CaO reactions with CO_2 and a typical sigmoid-type conversion curve, author empirically used a Boltzmann equation to fit the curves in the rapid reaction regime and obtained good simulation results.[9] No mechanism or model has described this feature during the initial nano-CaO carbonation reactions.

To establish a model of nano-CaO reactions with CO_2, we recently proposed an ion migration mechanism that was useful in explaining the diffusion of CO_2 in the $CaCO_3$ layer formed. Bathia[21] proposed that Ca^{+2} and CO_3^{-2} ions are predominant in $CaCO_3$ and that CO_3^{-2} is the mobile species in ionic conduction through $CaCO_3$. Furthermore, they

postulated that O^{-2} serves as a counter-current of a negatively charged species during the reaction process to maintain electroneutrality in the $CaCO_3$ product layer. The reaction, diffusion and movement actions are described in Eqs. 6–8

$$\text{At the pore surface: } CO_2(g) = (CO_2)_{ads} \tag{6}$$

$$(CO_2)_{ads} + O^{-2} \rightarrow CO_3^{-2} \tag{7}$$

$$\text{At the CaO} - \text{CaCO}_3 \text{ interface: } CO_3^{-2} + CaO = CaCO_3 + O^{-2} \tag{8}$$

Haul et al.[28,29] proposed that an isotopic exchange occurs between carbon dioxide and calcium carbonate. Yi et al.[30] chose to use mono-, bi-, and tri-metal oxides that possess oxygen vacancies as an additive of the CO_2 sorbent to provide a CO_2 diffusion pathway and facilitate O^{-2} ion migration.

In this study, a condition to distinguish between a rapid reaction regime and a slow reaction regime is proposed. Then, based on the ion migration hypotheses, a new ion reaction mechanism is proposed, and a kinetic model is developed for the rapid surface reaction of nano-CaO with CO_2. Finally, experiments were performed on the carbonation reaction of a sorption complex catalyst to examine and evaluate the kinetic model.

Model development

Based on the ion migration mechanism of CO_2 and CO_3^{-2} shown in Eqs. 6 and 7, the sorption of CO_2 is random on the surface of nano-CaO. The adsorption process may be described by an isothermal adsorption equation,[31,32] which is independent of the reaction conversion; thus, we proposed two hypotheses.

1. Bhatia[21] proposed that the formation and decomposition of CO_3^{-2} with O^{-2} was a possible pathway for effective CO_2 diffusion. Hence, we proposed that the formation and decomposition of CO_3^{-2} reaches equilibrium through the movement of CO_3^{-2} during the reactions and is described by Eq. 10.

2. Due to the stability of CaO, the reaction formation of CaO is a solid, while O^{-2} is the counter-current motion ion and is derived from the decomposition or the carbonation reaction.

We propose a new ion reaction mechanism of nano-CaO with CO_2 as presented in Eqs. 9–11.

$$\text{Adsorption on the surface: } CO_2(g) \rightleftharpoons (CO_2)_{ads} \tag{9}$$

$$(CO_2)_{ads} + O^{-2} \underset{k_2}{\overset{k_1}{\rightleftharpoons}} CO_3^{-2} \tag{10}$$

$$\text{Irreversible reaction : } CO_3^{-2} + CaO \xrightarrow{k_3} CaCO_3 + O^{-2} \tag{11}$$

In the experiments conducted in this research, the CO_2 concentration was far from the equilibrium concentration; thus, we speculate the carbonation reaction, Eq. 11, is irreversible. In the first stage, the initial product layer is small, and CO_2 has an extremely high diffusivity, causing the reaction at the CaO-$CaCO_3$ interface to be the control step.[24] Hence, we assume that Eq. 11 is the controlling reaction. From the derivation of the reaction kinetics, an elementary reaction assumption is used. Thus, the reaction kinetics equation of nano-CaO reacting with CO_2 is given by the following

$$r = k_3 \times \theta_{CO_3^{-2}} \times \theta_{CaO} \tag{12}$$

From Eq. 12, k_3 is the kinetic rate constant from Eq. 11, θ_{CaO} is the active CaO ratio on the catalyst surface and $\theta_{CO_3^{-2}}$ is the coverage ratio of CO_3^{-2} on the surface of the catalyst.

As expressed in hypothesis (1), because Eq. 10 reaches equilibrium and is an elementary reaction, it leads to Eq. 13

$$k_1 \times \theta_{(CO_2)_{ads}} \times \theta_{o^{-2}} = k_2 \times \theta_{CO_3^{-2}} \tag{13}$$

where k_1 and k_2 are the forward and reverse kinetic rate constants from Eq. 10, respectively, θ_{O}^{-2} is the coverage ratio of O^{-2} on the surface of the catalyst and $\theta_{(CO_2)ads}$ is the adsorption ratio of CO_2 on the surface of the catalyst.

By combining Eqs. 12 and 13, and defining $k' = \frac{k_1 \times k_3}{k_2}$, we obtain

$$r = k' \times \theta_{(CO_2)_{ads}} \times \theta_{CaO}{}' \times \theta_{O^{-2}} \tag{14}$$

From Eq. 14, $\theta_{(CO_2)ads}$ presents the isothermal adsorption behavior of CO_2 from Eq. 9, which can be obtained by the Langmuir, Temkin, or Freundich isothermal adsorption equations. In this study, the Temkin isothermal adsorption equation is more suitable to describe the chemical adsorption characteristics of CaO and CO_2 because of the exponential relationship between the adsorption active energy and adsorption capacity. This relationship can be expressed as follows

$$\theta_{(CO_2)_{ads}} = b \times \ln(a \times P) \tag{15}$$

where a is a function of temperature, b is a constant and $\theta_{(CO_2)\text{ads}}$ is the coverage ratio of CO_2 on the surface of CaO.

The variables θ_O^{-2} and θ_{CaO} can be obtained by simplifying the ion migration hypothesis. Based on hypothesis (1), we assume that the mole number of O^{-2} in the sorbent is proportional to the mole number of $CO_3{}^{-2}$ ions or $CaCO_3$ formed. For the local reaction area, if we set the mole number of reacted CaO as N_1, the mole number of unreacted active sites of CaO on the surface as N_2, the total CaO mole number on the surface as N, and the mole number of O^{-2} ions is proportional to the number of reacted CaO, where C is proposed as the proportionality coefficient, a constant, then we obtain the following equations

$$N_1 + N_2 = N \tag{16}$$

Hence

$$\theta_{O^{-2}} = \frac{CN_1}{N} \tag{17}$$

$$\theta_{CaO} = \frac{N_2}{N} \tag{18}$$

For the adsorbent, if we assume that n is the mole number of CaO in the sorbent, X is the conversion of CaO, and X_u is the ultimate conversion of CaO in the rapid reaction regime, then the conversion X and X_u can be expressed as follows

$$X = \frac{N_1}{n} \tag{19}$$

$$X_u = \frac{N}{n} \tag{20}$$

Substituting Eqs. 16–20 in Eq. 14, we can express the rate as Eq. 21

$$r = k' \times C \times \theta_{(CO_2)ads} \times \frac{X}{X_u}\left(1 - \frac{X}{X_u}\right) \tag{21}$$

The reaction rate can also be expressed as Eq. 22

$$r_1 = \frac{dN_1}{dt} \tag{22}$$

Introducing Eq. 19 in Eq. 22, we obtain Eq. 23

$$r_1 = n\frac{dX}{dt} \tag{23}$$

n is a constant in a reaction; therefore, we obtain a varied type of the reaction rate

$$r = \frac{dX}{dt} \tag{24}$$

$$\text{Thus, } r = \frac{dX}{dt} = k \times \frac{X}{X_u}\left(1 - \frac{X}{X_u}\right) \tag{25}$$

where

$$k = k'C\theta_{(CO_2)ads} \tag{26}$$

The differential equation expressed in Eq. 25 is as follows

$$\frac{dr}{dt} = \frac{d^2X}{dt^2} = \frac{k}{{X_u}^2}(X_u - 2X)\frac{dX}{dt} \tag{27}$$

When $dr/dt = d^2X/dt^2 = 0$, it is related to the point of r_{max}; we define this related conversion point as X_1, and we obtain $X_1 = 1/2X_u$.

From Eqs. 25 and 27, the reaction rate variation with time is nonmonotonic and reaches a maximum (r_{max}) when the conversion X is half of the ultimate conversion X_u in the chemical reaction control regime. The experimental results of the two curves are shown in Figure 1: the conversion X vs. the time t curve (the dashed curve) and the reaction rate dX/dt vs. t curve (the solid curve). The left vertical axis represents the reaction conversion X, and the right vertical axis represents the reaction rate dX/dt. There is a maximum reaction rate, r_{max}, determined by the point of $d^2X/dt^2 = 0$, and related to the conversion X_1. When we obtain the conversion X_1, we can calculate the ultimate conversion X_u. Furthermore, we proposed a criterion when the conversion point of X increased to X_u, as shown in Figure 1. X_u is the critical point that divides the reaction into a rapid reaction regime and a slow reaction regime. When $X \le X_u$, the reaction is a rapid reaction regime, and when $X > X_u$, it is a slow reaction regime.

From Figure 1, we define the time with the point of $dr/dt = 0$ or $X_1 = X_u/2$ as t_0. Using the initial conditions below and integrating Eq. 25 for the area of [0, t_0] and [t_0, t], we obtain the final integral equation

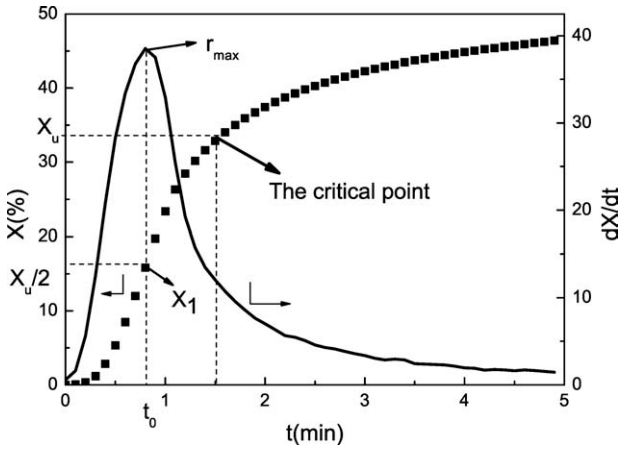

Figure 1. The curves of conversion and derivative of nano-CaO in the sorption complex catalyst.

The carbonation temperature was 823 K, and the P_{CO_2} was 0.016 MPa.

$$\begin{aligned} 0 < t \le t_0 &: t = t,\ X = X \\ &\quad t = t_0,\ X = X_1 = 1/2X_u \\ t_0 \le t &: t = t_0,\ X = X_1 = 1/2X_u \\ &\quad t = t,\ X = X \\ X &= X_u - \frac{X_u}{1 + \exp\left[\frac{(t-t_0)k}{X_u}\right]} \quad (0<X\le X_u) \end{aligned} \tag{28}$$

Equation 28 is very similar to the Boltzmann equation and represents sigmoid-type conversion curves. When $t < t_0$, dX/dt increases; however, when $t > t_0$, dX/dt decreases with increasing time. When $X > X_u$, the reaction enters the slow reaction regime. The layer of $CaCO_3$ formed by rapid carbonation dominates the carbonation rate. The kinetics of the slow reaction section is the same as other models for micro-CaO reacting with CO_2.

The reason for the sigmoid-type conversion curves in the rapid surface reaction regime shown in Figure 1 is the diffusion rate of CO_2 and the amount of unreacted nano-CaO. The process can be explained by the ion reaction mechanism of Eqs. 10 and 11. At the beginning of the reaction, the diffusion rate of CO_2 in the gas phase is fast, and much of the ${CO_3}^{-2}$ forms according to Eq. 10. This process simultaneously accelerates the CaO carbonation reaction of Eq. 11 to form $CaCO_3$. After a short reaction time, the conversion rate is lower because the amount of unreacted nano-CaO is decreased. A layer of $CaCO_3$ may not form during the rapid surface reaction regime. After a layer of $CaCO_3$ is formed, CO_2 diffusion through the $CaCO_3$ becomes the rate-limiting step. The mechanism and model for CO_2 diffusion is similar to the micro-CaO reaction with CO_2, which is not addressed in this article.

Experimental

To evaluate the model, a sorption complex catalyst, containing nano-CaO as the CO_2 adsorbent and Ni as the

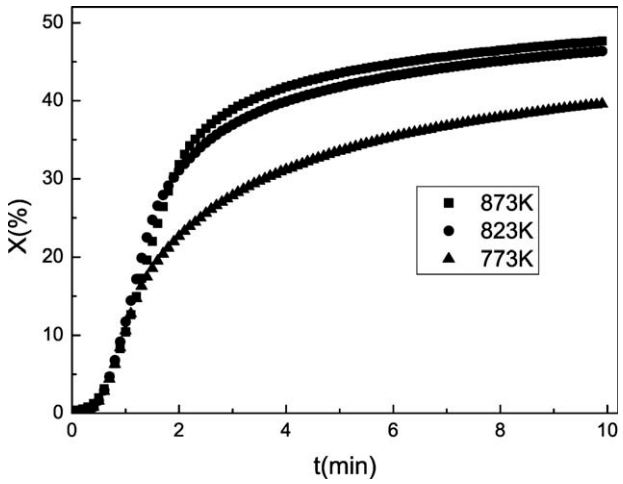

Figure 2. Conversion of nano-CaO carbonation in the sorption complex catalyst.

The carbonation temperatures were 773, 823, and 873 K, respectively, and the P_{CO_2} was 0.012 MPa.

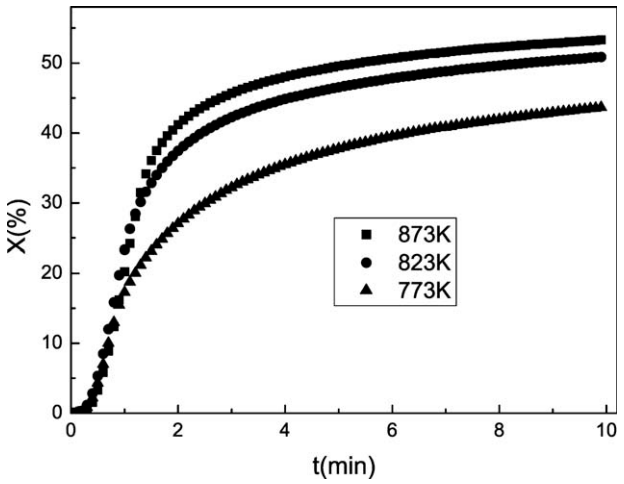

Figure 4. Conversion of nano-CaO carbonation in the sorption complex catalyst.

The carbonation temperatures were 773, 823, and 873 K, respectively, and the P_{CO_2} was 0.016 MPa.

reforming catalyst, was prepared. Nano-$CaCO_3$ powder with a particle size of 70 nm (Huzhou Linghua, China) was used as the nano-CaO precursor. The content of nano-$CaCO_3$ in the complex was ~50%.

A thermogravimetric analyzer (Pyris1TGA, Perkin–Elmer) was used to study the carbonation reaction kinetics of nano-CaO reacting with CO_2 in the sorption complex catalyst. Approximately 3 mg of catalyst complex was used in the sample holder to avoid interparticle diffusion effects in the platinum basket. The complex was calcined for 10 min at 1003 K in a N_2 atmosphere with a gas flow rate of 46 ml/min. The temperature was then decreased to the designated reactive temperature, and CO_2 gas was introduced to obtain an atmosphere with the designed CO_2 partial pressure. The carbonation reaction was studied over a temperature range of 773–873 K, and the CO_2 partial pressure P_{CO_2} was varied between 0.012 and 0.020 MPa. Based on the CO_2 content of normal industrial applications, we selected a CO_2 partial pressure of 0.012, 0.014, 0.016, or 0.020 MPa. The carrier gas was nitrogen. The reasons for selecting this range of reaction temperatures and CO_2 partial pressures were the industrial need and the results of previous studies.

Experimental results and discussions

Figures 2–5 show the carbonation conversions of the nano-CaO in the sorption complex catalyst with time under the partial pressures of CO_2 of 0.012, 0.014, 0.016, and 0.020 MPa at the different temperatures of 773, 823, and 873 K, respectively. The carbonation conversion, X, of nano-CaO varied with the temperature and CO_2 partial pressure.

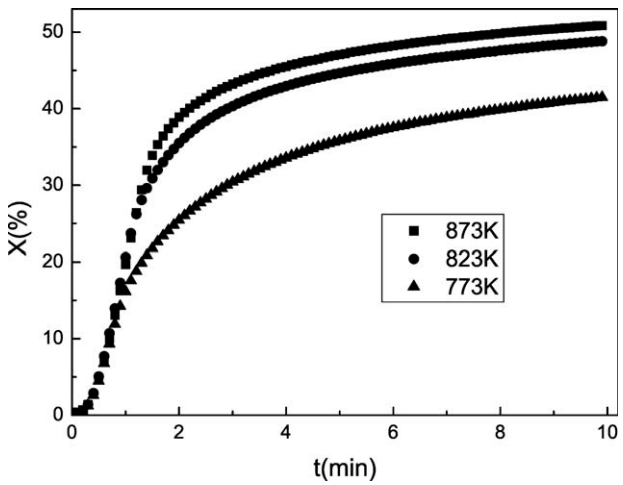

Figure 3. Conversion of nano-CaO carbonation in the sorption complex catalyst.

The carbonation temperatures were 773, 823, and 873 K, respectively, and the P_{CO_2} was 0.014 MPa.

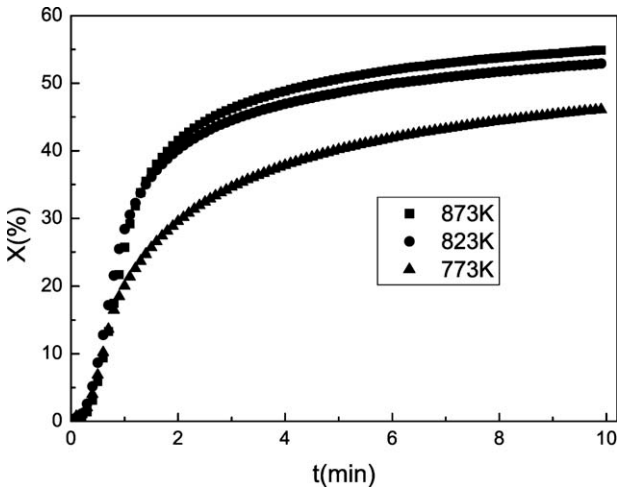

Figure 5. Conversion of nano-CaO carbonation in the sorption complex catalyst.

The carbonation temperatures were 773, 823, and 873 K, respectively, and the P_{CO_2} was 0.020 MPa.

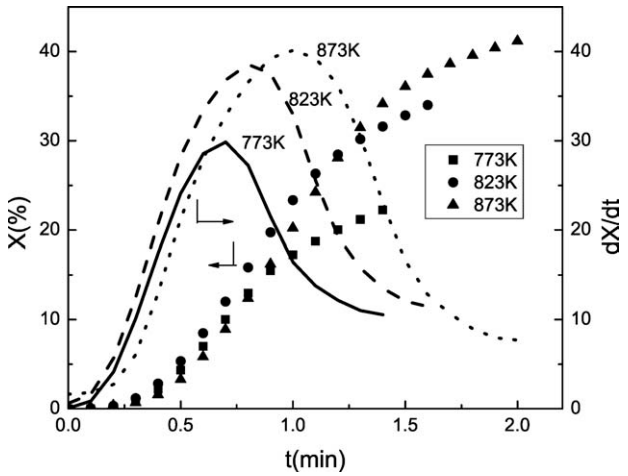

Figure 6. *dX/dt-t* curves of nano-CaO carbonation in the sorption complex catalyst.

The carbonation temperatures were 773, 823, and 873 K, respectively, and the P_{CO_2} was 0.016 MPa.

The curves represent typical sigmoid curves, similar to nano-CaO reactions with CO_2 in CaO/Al_2O_3 sorbents described in other published work related to the carbonation reaction.[9]

Figures 6 and 7 show the sigmoid X vs. t curves and the nonmonotonic r (dX/dt) vs. t curves at the first 2 minutes of the fast reaction sections for different temperatures and CO_2 partial pressures. The left coordinate axis represents the reaction conversion X, and the right axis represents the reaction rate r (dX/dt). From Figures 6 and 7, sigmoid-type curves are obvious, and each curve appears to be a peak. Each peak relates to an r_{max} point, and the sigmoid-shaped curves relate to the X curve in Figures 6 and 7. Figure 6 shows that as temperature increased, both t_0 and r_{max} increased. The reaction rate at 873 K was higher than that at the other two temperatures. Figure 7 shows that as the carbonation rate increased and the reaction time (t_0) increased, the CO_2 partial pressure also increased.

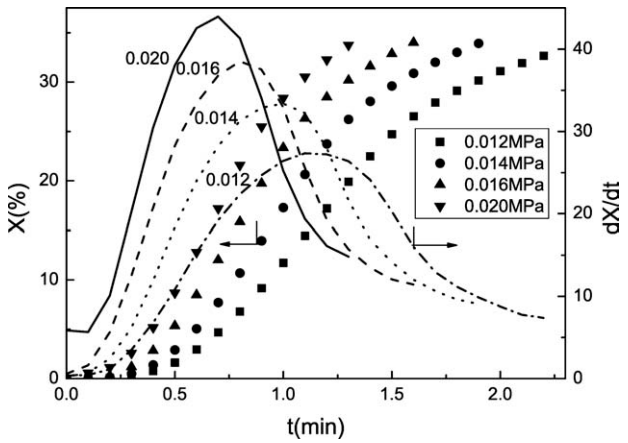

Figure 7. *dX/dt-t* curves of nano-CaO carbonation in the sorption complex catalyst.

The carbonation temperature was 823 K, and the P_{CO_2}, was 0.012, 0.014, 0.016, and 0.020 MPa, respectively.

Table 1. The Vales of X_u Under the Various Conditions

P_{CO2} (MPa)	773 K	823 K	873 K
0.020	21.90	34.16	41.28
0.016	21.80	33.89	40.86
0.014	22.00	33.51	39.31
0.012	22.05	32.02	38.71

The variables X_u, t_0, and k in Eq. 28 change with the reaction temperature or CO_2 partial pressures. The results from Figures 2–5 of the carbonation conversion were fitted using Origin software to determine the parameters X_u, t_0, and k.

Estimation of X_u

From the experimental results shown in the Table 1, the ultimate conversion of the rapid reaction regime, X_u, was found to be first order with respect to the reaction temperature (773–873 K). Thus, a linear equation, Eq. 29, was used to empirically express X_u for CaO carbonation conversion

$$X_u = -118.09 + 0.18T \quad (773.\mathrm{K} \le T \le 873.\mathrm{K}) \tag{29}$$

Similar methods were used in the empirical carbonation conversion equations. Li[33] also found that the ultimate conversion of CaO was independent of the CO_2 fraction but increased linearly with increasing reaction temperatures (873–973 K). Lee[34] proposed that the total ultimate conversion be expressed as a function of k, which is a kinetic rate constant.

Apparently, a higher temperature promotes the reaction of CaO with CO_2 resulting in a higher ultimate conversion during the kinetically-controlled reaction regime. Higher temperatures may also accelerate the diffusion of the CO_3^{-2} and O^{-2} ions in the $CaCO_3$ layer. This phenomenon is supported by Alvarez and Abanades,[35] who showed that the critical thickness of the product layer affected the apparent ultimate conversion. In addition, higher temperatures promoted the endothermic reaction of CaO carbonation.

Estimation of t_0

Figures 6 and 7 show that an increase in the partial pressure of CO_2 in the atmosphere or a decrease in the reaction temperature has the same effect as decreasing the time required to reach the maximum reaction rate t_0. However, the higher partial pressure of CO_2 caused an increase in the amount of CaO conversion, and lower reaction temperatures caused a decreased conversion. Increasing the CO_2 partial pressure increased the CO_2 equilibrium adsorption amount, and increasing the temperature should promote the endothermic reaction of CaO with CO_2. Thus, both temperature and CO_2 partial pressure were used to estimate t_0 using the least square method, as shown empirically in Eq. 30

$$t_0 = -0.57 + 0.29T/100 - 58.16P_{CO_2} \tag{30}$$

The unit of the reaction temperature T is K, and the unit of the CO_2 partial pressure, P_{CO_2}, is MPa. Equation 30 is valid when 773 K $\le T \le$ 873 K and 0.012 MPa $\le P_{CO_2} \le$ 0.02 MPa.

Estimation of k

The Temkin isothermal adsorption equation was introduced in Eq. 26. The constant b is a temperature-independent constant. Using this constant, Eq. 31 was derived

$$k = k_4 \times \ln(a \times P_{CO_2}) \tag{31}$$

In this equation, $k_4 = k'$ Cb, where C and b are independent of temperature.

An Arrhenius plot was constructed for individual values of k_4 obtained from the fitted result at various temperatures. The value of the activation energy E was 30.2 kJ/mol, and k_4 was obtained using Eq. 32

$$k_4 = 11.5723 \times 10^3 \times \exp\left(-\frac{30.2 \times 10^3}{8.314T}\right) \tag{32}$$

Although the constant decreased steadily as the temperature increased, the relationship between the parameter, a, and the temperature, T, was not suitable for the Arrhenius equation. As a result, an empirical equation was derived

$$a = -444.13 + 1.17T - 7.39 \times \left(\frac{T}{100}\right)^2 \tag{33}$$

Based on the discussion above, the effects of k can be characterized as either the kinetic reaction rate or the CO_2 adsorption capacity. This contradictory relationship weakened the influence of temperature on the apparent reaction rate. In some cases, including those presented by Bhatia,[21] Li,[33] and Dennis,[36] temperature did not affect the apparent reaction rate.

Temperature may affect the kinetic constant in the Arrhenius equation; however, higher temperatures could lead to more active CaO, as discussed in sections above. The equilibrium adsorption amount decreased, and as a result, the negative effect of high temperature on the equilibrium adsorption amount made the apparent kinetic constant, k_4, irregular with regard to temperature in the Arrhenius equation.

Thus, the rapid carbonation kinetic model of nano-CaO in the sorption complex catalyst is presented as

$$X = X_u - \frac{X_u}{1 + \exp\left[\frac{(t - t_0)k}{X_u}\right]} \tag{28}$$

where, $X_u = -118.09 + 0.18\mathrm{T}$

$$t_0 = -0.57 + 0.29T/100 - 58.16P_{CO_2}$$

$$k = 11.572 \times 10^3 \times \exp\left(-\frac{30.2 \times 10^3}{8.314T}\right) \times \ln(a \times P_{CO_2})$$

$$a = -444.13 + 1.17T - 7.39 \times \left(\frac{T}{100}\right)^2$$

(773 K$\leq T \leq$873 K, 0.012 MPa$\leq P_{CO_2} \leq$0.02 MPa).

Model examination

Figure 8 shows a comparison of the predicted and the experimental data in the kinetically controlled region from the carbonation conversions derived from Eq. 28. The average relative deviation was less than 9.86% when the carbonation conversion was greater than 3%. When the conversion was less than 3%, the average value of the absolute errors was 0.77%, and the maximum of the absolute error was 1.83%. It appears that the kinetic model derived in this article accurately depicts the carbonation kinetics of a sorption complex catalyst. Furthermore, the X-t sigmoid-type curve of nano-CaO reactions with CO_2 can be represented by the kinetic model in Eq. 28.

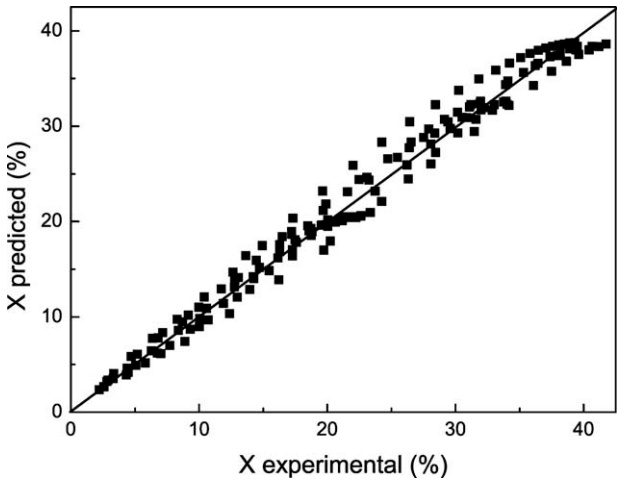

Figure 8. Comparisons of predicted and experimental data for carbonation conversion.

Conclusions

Based on the hypotheses of ion migration, a new ion reaction mechanism of nano-CaO reacting with CO_2 has been proposed. A new condition to distinguish between rapid surface reactions and slow diffusion reactions of nano-CaO with CO_2 was proposed. A kinetic model in the form of the Boltzman equation was developed for the first time. The kinetic model is in agreement with the characteristics of the carbonation reaction of nano-CaO with CO_2 in the kinetically controlled reaction regime. The experimental carbonation reaction curves were successfully described by the kinetic model of a sorption complex catalyst at temperatures of 773–873 K and CO_2 partial pressures of 0.012 and 0.020 MPa. The activation energy during carbonation was estimated to be 30.2 kJ/mol. The average relative deviation of carbonation in the rapid kinetic control reaction regime was less than 9.8%.

Acknowledgments

The authors are grateful to the National Natural Science Foundation of China (20876142) and to the China High technology ministry 863 program (2009AA05Z104) for financial support.

Notation

a = parameter in the Temkin isothermal adsorption equation
b = constant in the Temkin isothermal adsorption equation
C = proportional coefficient, a constant
C_{CO2} = concentration of CO_2
D = diffusion coefficient
E = activation energy
k = kinetic rate constant in Eq. 28

k_1 and k_2 = kinetic rate constants of the reaction in Eq. 11
k_3 = kinetic rate constant of the reaction in Eq. 12
k_4 = parameter in Eq. 31
k' = effective kinetic rate constant in Eq. 15
K = kinetic rate constant in Eqs. 2, 4, and 5
L_0 = initial total pore length in the porous system per unit of volume
n = mole number of CaO in the sorbent
N = mole number of the total CaO on the surface
N_1 = mole number of reacted CaO on the surface
N_2 = number of unreacted active sites of CaO on the surface
P_{CO_2} = partial pressure of CO_2 in the reaction atmosphere
S_0 = initial surface area per unit volume
t = carbonation reaction time
t_0 = reaction time related to the maximum conversion rate
T = reaction temperature
X = conversion of CaO
X_1 = conversion of CaO related to the maximum conversion rate
X_u = ultimate conversion of CaO in the rapid reaction region

Greek letters

ε_0 = initial porosity
$\theta_{(CO_2)ads}$ = coverage ratio of CO_2 on the surface of CaO
$\theta_{O^{-2}}$ = coverage ratio of O^{-2} on the surface of the catalyst
$\theta_{CO_3^{-2}}$ = coverage ratio of CO_3^{-2} on the surface of the catalyst
θ_{CaO} = active CaO ratio on the catalyst surface
ψ = structural parameter

Literature Cited

1. Harrison DP. Sorption-enhanced hydrogen production: a review. *Ind Eng Chem Res*. 2008;47:6486–6501.
2. Han C, Harrison DP. Simulation shift reaction and carbon dioxide separation for the direct production of hydrogen. *Chem Eng Sci*. 1994;49:5875–5883.
3. Hufton JR, Mayorga S, Sircar S. Sorption-enhanced reaction process for hydrogen production. *AIChE J*. 1999;45:248–256.
4. Ding Y, Alpay E. Adsorption-enhanced steam-methane reforming. *Chem Eng Sci*. 2000;55:3929–3940.
5. Xiu G, Li P. Sorption enhanced reaction process with reactive regeneration. *Chem Eng Sci*. 2002;57:3893–3908.
6. Wu SF, Li LB, Zhu YQ, Wang XQ. A micro-sphere catalyst complex with nano $CaCO_3$ precursor for hydrogen production used in ReSER process. *Eng Sci*. 2010;8:22–26.
7. Wu SF, Li QH, Kim JN, Yi KB. Properties of a nano CaO/Al_2O_3 CO_2 sorbent. *Ind Eng Chem Res*. 2008;47:180–184.
8. Wu SF, Zhu YQ. Behavior of $CaTiO_3$/nano-CaO as a CO_2 reactive adsorbent. *Ind Eng Chem Res*. 2010;49:2701–2706.
9. Shi Q, Wu SF, Jiang MZ, Li QH. Reactive sorption-decomposition kinetics of nano Ca-based CO_2 sorbents. *CIESC J*. 2009;60:641–648.
10. Wu SF, Beum TH, Yang JI, Kim JN. The characteristics of a sorbent-enhanced steam-methane reaction for the production of hydrogen using CO_2 sorbent. *Chin J Chem Eng*. 2005;13:43–47.
11. Lee DK, Baek II H, Yoon WL. Modeling and simulation for the methane steam reforming enhanced by in situ CO_2 removal utilizing the CaO carbonation for H_2 production. *Chem Eng Sci*. 2004;59:931–942.
12. He J, Wu SF. The characteristics of sorption enhanced steam methane reforming for hydrogen production on a complex catalyst. *Chem React Eng Technol (China)*. 2007;23:470–373.
13. Johnsena K, Ryub HJ, Grace JR, Lim CJ. Sorption-enhanced steam reforming of methane in a fiuidized bed reactor with dolomite as CO_2-acceptor. *Chem Eng Sci*. 2006;61:1195–1202.
14. Johnsen K, Grace JR, Elnashaie SSEH, Kolbeinsen L, Eriksen D. Modeling of sorption-enhanced steam reforming in a dual fluidized bubbling bed reactor. *Ind Eng Chem Res*. 2006;45:4133–4144.
15. Gupta H, Fan LS. Carbonation-calcination cycle using high reactivity calcium oxide for carbon dioxide separation from flue gas. *Ind Eng Chem Res*.2002;41:4035–4042.
16. Abanades JC, Anthony EJ, Lu DY, Salvador C, Alvarez D. Capture of CO_2 from combustion gases in a fluidized bed of CaO. *AIChE J*. 2004;50:1614–1622.
17. Lu DY, Hughes RW, Anthony EJ. Ca-based sorbent looping combustion for CO_2 capture in pilot-scale dual fluidized beds. *Fuel Process Technol*. 2008;89:1386–1395.
18. Fang F, Li ZS, Cai NS. Continuous CO_2 capture from flue gases using a dual fluidized bed reactor with calcium-based sorbent. *Ind Eng Chem Res*. 2009;48:11140–11147.
19. Bhatia SK, Perlmutter DD. A random pore model for fluid-solid reactions: I. Isothermal, kinetic control. *AIChE J*. 1980;26:379–386.
20. Bhatia SK, Perlmutter DD. A random pore model for fluid-solid reactions: II. Diffusion and transport effects. *AIChE J*. 1981;27:247–254.
21. Bhatia SK, Perlmuter DD. Effect of the product layer on the kinetics of the CO_2-lime reaction. *AIChE J*. 1983;29:79–86.
22. Wu SF, Li QH. *Adsorption kinetics of nano CaO base CO_2 adsorbent. Presented at the 5th International Conference on Separation Science and Technology*, Beijing, China, 2007: 14–16.
23. Florin NH, Harri AT. Reactivity of CaO derived from nano-sized $CaCO_3$ particles through multiple CO_2 capture-and-releasecycles. *Chem Eng Sci*. 2009;64:187–191.
24. Lu H, Khan A, Pratsinis SE, Smirniotis PG. Flame-made durable doped-CaO nanosorbents for CO_2 capture. *Energy Fuels*. 2009;23:1093–1100.
25. Chen GT. Chemical Reaction Engineering, 2nd ed. Hangzhou: Chemical Industry Press,1990:171–173.
26. Sun P, Grace JR, Lim CJ, Anthony EJ. A discrete-pore-size-distribution-based gas-solid model and its application to the $CaO+CO_2$ reaction. *Chem Eng Sci*. 2008;63:57–70.
27. Grasa G, Murillo R, Alonso M, Abanades JC. Application of the random pore model to the carbonation cyclic reaction. *AIChE J*. 2009;55:1264–1255.
28. Haul RAW, Stein LH, Devilhers JWL. Exchange of carbon-13 dioxide between calcite crystals and gaseous carbon dioxides. *Nature*.1953;171:619.
29. Haul RAW, Stein LH. Diffusion in calcite crystals on the basis of isotopic exchange with carbon dioxide. *Trans Faraday Soc*.1955;51:1280.
30. Yi KB, Ko CH, Park JH, Kim JN. Improvement of the cyclic stability of high temperature CO_2 absorbent by the addition of oxygen vacancy possessing material. *Catal Today*. 2009;146:241–247.
31. Ramachandran PA. Analysis of non-catalytic reaction following Langmiur-Hinshelwood kinetic. *Chem Eng J*.1982;23:223–225.
32. Sohn H, Szekely J. A structural model for gas-solid reactions with a moving boundary—IV. Langmuir-Hinshelwood kinetics. *Chem Eng Sci*. 1973;28:1169–1177.
33. Li ZS, Cai NS. Modeling of multiple cycles for sorption-enhanced steam methane reforming and sorbent regeneration in fixed bed reactor. *Energy Fuels*. 2007;21:2909–2918.
34. Lee DK. An apparent kinetic model for the carbonation of calcium oxide by carbon dioxide. *Chem Eng J*. 2004;100:71–77.
35. Alvarez D, Abanades JC. Determination of the critical product layer thickness in the reaction of CaO with CO_2. *Ind Eng Chem Res*. 2005;44:5608–5615.
36. Dennis JS, Hayhurst AN. The effect of CO_2 on the kinetics and extent of calcination of limestone and dolomite particles in fluidized beds. *Chem Eng Sci*. 1987;42:2361–2372.

Manuscript received Oct. 20, 2010, revision received Feb. 3, 2011, and final revision received May 2, 2011.